STUDY OF COMPLEXATION OF TRANSITION METALS USING DISSIPATIVE PARTICLE DYNAMICS AND ITS APPLICATION TO REAL SYSTEM

By RAVISH KUMAR

A thesis submitted to the

Graduate School – New Brunswick

Rutgers, The State University of New Jersey

In partial fulfillment of the requirement

For the degree of

Master of Science

Graduate Program in Chemical and Biochemical Engineering

Written under the direction of

Dr. Alexander V. Neimark

And approved by

_____

_____

_____

_____

New Brunswick, New Jersey

May, 2017

ABSTRACT OF THE THESIS

STUDY OF COMPLEXATION OF TRANSITION METALS USING DISSIPATIVE PARTICLE DYNAMICS AND ITS APPLICATION TO A REAL SYSTEM

By RAVISH KUMAR

Thesis Director:

Dr. Alexander V. Neimark

This work aims at developing a methodology that allows application of coarse-grained simulation techniques to systems with reactive equilibria. In particular, we apply dissipative particle dynamics, a simple but computationally efficient technique where components are represented by beads interacting with soft short-range potentials to solutions containing transition metal ions. A transition metal ion is presented by a cluster of beads: one central bead and several "coordination vacancies" arranged around the central one according to complexation geometry characteristic to that particular metal; that geometry is maintained using a system of covalent bonds and angles. The beads representing coordination vacancies are able to form dissociable Morse bonds with the ligand beads. The strength, length and lifetime of the bonds are regulated by the Morse parameters. After introducing the approach, we study the basic properties of the model, namely the number and stability of complexi in solutions formed by a metal salt and one or two ligands. Then, we apply the model to a practical system: transition metal chloride in polyvinylpyrrolidone - dimethylformamide solution. We studied the Poiseuille flow of the solution

and its dependence on the transition metal concentration, solvent composition, polymer length, and the driving field. We attempted to reproduce experimental data on the dependence of dynamic properties on the composition.

ACKNOWLEDGMENT

It is with immense gratitude that I acknowledge the support and help of my advisors, Professor Alexander V. Neimark and Dr. Aleksey Vishnyakov, whose encouragement, insightful guidance and great support during my M.S. study helped me to complete my research project. It is my honour to have the opportunity to study molecular simulation in their group. This research would not have been possible without their invaluable advice, support and their enormous patience throughout my time at Rutgers University. I believe that everything that I learned here today will benefit my life in the future.

I am also heartily thankful to Dr. Ming-Tsung Lee, a former PhD candidate in Professor Neimark's research group. He guided me and gave insightful suggestions about coding, algorithm and technical details for the simulation and also for helping me establish a basic foothold in the project and providing astute assessment of my work which helped me proceed forward.

Furthermore, I would like to thank professor Dr. Meenakshi Dutt for being my committee member and providing invaluable advice on my work.

This work was supported by ACS PRF grant 54610 ND6 "Mesoscale simulation of asphaltene aggregation in crude oil".

Finally, I take this opportunity to convey my sincere thanks to my loving parents, my group members, and all of my friends who supported me in any respect during my master's thesis study.

Table of Contents

List of Tables

List of Illustrations

1 Introduction

1.1 Historical overview: DPD and its application to reactive systems.

Computer simulations have beyond doubt become one of the most important research tools in modern physics. They bridge experiment and theory. They are especially useful in predictions of materials behavior at unusual conditions such as high temperature and pressure or at conditions which are difficult to achieve experimentally. One such method, Monte Carlo method is handy when only equilibrium properties are required but is very limited in studies of dynamic properties. And Molecular Dynamics (MD) considers motion of molecules in real time and therefore is more applicable to dynamic behavior. Even though MC and MD simulations nowadays can handle millions of molecules due to increase in computer power, atomistic models are still limited in terms of spatial and temporal scales they can access. For large systems with macromolecules like polymers, mesoscale methods have been developed with cruder, more approximate force fields. Molecules are presented as collections of quasiparticles or “beads”; development of such models is known as “coarse graining”. This method extend the time and scale at the cost of electronic and atomic detail. Coarse graining reduces the number of interaction centers and thus intermolecular pair interaction between molecules. This enables us to apply on larger system and also enabling longer time scales. It provides more insight into qualitative behavior rather than quantitative results. One of the most popular coarse-grained technique is dissipative particle dynamics (DPD), which uses short-range and repulsive potentials between the beads. Besides conservative forces, the beads interact via random and drag forces (also soft and short-ranged). By solving Langevin equations of beads motion, we can analyze the behavior of the system. Short and soft interactions make DPD extremely efficient computationally, at the expense of model crudeness, which, of course, limits its applicability.

DPD has been applied to a large variety of systems, including simple fluids, linear homopolymers[1], block[2] and random copolymers[3], lipids[4], DNA[5], and proteins[6]. Despite model crudeness DPD has also been applied to reactive systems. For polymerization reactions, insertion and removal of polymer chains are required. Lisal et al[7, 8] have developed reaction ensemble dissipative particle dynamics method for studying the reaction equilibrium of polymer melts. The reaction ensemble enabled studies of the effect of polydispercy of polymer chains that was considered using DPD for the first time. The association and dissociation of bonds was introduced using Monte Carlo style novels integrated into the DPD algorithm. Formation and breakup of temporary bonds was considered also by Karimi-Varzaneh et al [9], with a purpose of mimicking polymer chain entanglements in polymer solutions and melts. Although their focus was on polymer melt viscosity with soft core model, their approach is relevant to reactive system as well. Nikoubashman et al[10] numerically studied phase behavior of block polymers of equal molecular weight confined in thin films. Formation and breakup of temporary bonds enabled mesoscale modeling of double-stranded DNA[11]. Similar concept was employed to represent protein structures: a system of forming/dissociated bonds enables DPD simulations of formation α– helixes and β-loops of peptides[6].

Next step in extending DPD applicability was its application to system with protonation – deprotonation equilibria. For this purpose, one needs a DPD model of proton. Lee et al[12] introduced proton as a bead with charge on it which formed dissociable bond with base beads, namely neutral water bead and charged sulfonate. Protons had no short -range repulsion with base beads but were repelled from hydrophobic beads. They applied Morse potential cut and shifted to zero at cut off distance. Because of Morse potential applied protons and bases formed intermediate complexi so that proton could hop between the base beads, which mimicked artificially Grotthuss diffusion mechanism. This hopping frequency was controlled by Morse

potential parameters, which were adjusted accordingly. Application of this to simulate proton mobility and reaction equilibria between protonated and deprotonated acid forms in aqueous solutions was possible due to this concept. There was quantitative agreement with the experiments for proton self-diffusion coefficient and hopping frequency and also with the degree of dissociation of benzenesulfonic acid.

This method was further extended to study nanoscale segregation, water diffusion and proton conductivity in hydrated sulfonated polystyrene (sPS)[13]. The Morse potential was again applied to mimic the hopping of proton between bases and water. Again coarse grained modeling included short-range soft repulsion and smeared charge electrostatic potentials[14] to represent polymer and water. The polymer and water were modeled by coarse-grained beads interacting via short-range soft repulsion and smeared charge electrostatic potentials. Morse bond formation and breakup artificially mimics the Grotthuss mechanism of proton hopping between the bases (water and sulfonates). General DPD model was adopted to parameterize beads and volumes were taken from Bondi table [15] data used in UNIFAC [16]. Parameterization was done by matching the proton mobility in bulk water, dissociation constant of benzenesulfonic acid and liquid-liquid equilibrium of water-ethylbenzene solutions. Nanoscale segregation in the hydrated sPS into hydrophobic and hydrophilic subphases, water self diffusion, and proton mobility was predicted by the DPD simulations semi-quantitatively. The system was modeled at different hydration levels. With the increase of hydration there was transition from water clusters to 3D network of transport channels. This dynamic percolation effect of formation and breakup of temporary junctions between water clusters has been demonstrated by the analysis of hydrophilic subphase connectivity and water diffusion. Prediction of proton and water diffusion and its dependence on the hydration level has been compared with the experimental results and they were reasonably in agreement.

In this work, DPD is extended onto systems that feature complexation, that is, formation of coordination bonds between a transition metal and ligands. The methodology is somewhat similar to that developed for acids: transition metal is presented as cluster of beads, which forms dissociable Morse bonds with ligands beads. As a characteristic system, we selected metal chloride- polyvinylpyrrolidone (PVP) - dimethylformamide (DMF) system. The metal ion has four coordination position two of which are occupied by chloride anions and therefore the complex is neutrally charged. The remaining two positions are available for ligands to bind, and both PVP monomers and DMF qualify as ligands.

2 Simulation techniques and coarse-grained models

2.1 Dissipative Particle Dynamics simulation method

In a standard DPD simulation, the movement of bead is governed via pairwise interaction, including conservative soft repulsive, random, drag, bond, and electrostatic forces. The system dynamics and equilibrium are studied by solving Newton's equation of motions with pairwise interbead forces :

$$\mathrm{F}_{ij}(\mathrm{r}_{ij)}) = \mathrm{F}_{ij}^{\mathrm{C}}(\mathrm{r}_{ij}) + \mathrm{F}_{ij}^{\mathrm{B}}(r_{ij}) + \mathrm{F}_{ij}^{\mathrm{R}}(\mathrm{r}_{ij}) + \mathrm{F}_{ij}^{\mathrm{D}}(\mathrm{r}_{ij}, \mathrm{v}_{ij}) + \mathrm{F}_{ij}^{(\mathrm{M})}(\mathrm{r}_{ij}) \quad (1)$$

All beads are assigned an equal effective diameter R_c. The soft repulsion force acts between overlapping beads:

$$\mathrm{F}_{ij}^{\mathrm{C}}(\mathrm{r}_{ij}) = \mathrm{a}_{ij}\left(1 - \frac{\mathrm{r}_{ij}}{R_c}\right)\mathrm{r}_{ij}/\mathrm{r}_{ij} \quad (2)$$

at $r < R_c$, at $r \geq R_c$, where a_{ij} is the repulsion parameter specific to the given bead pair of types i and j. Following the standard approach to DPD simulations of self-assembly[17], the intra-component repulsion parameters a_{ii} between beads of the same type are set equal, irrespective to the bead type. The beads are tightly packed with a substantial overlap. We accepted the reduced bead packing density of ρR_c^3=3, common in DPD simulations[17].

The random and drag forces also acted between overlapping beads along the line connecting the bead centers. Random force that accounts for thermal fluctuations, is taken proportional to the conservative force that is also acting along the vector between the bead centers:

$$\mathrm{F}_{ij}{}^{(\mathrm{R})}(\mathrm{r}_{ij}) = \sigma w^{\mathrm{R}}\Theta_{ij}(t)\mathrm{r}_{ij} \quad (3)$$

where $\Theta_{ij}(t)$ is a randomly fluctuating in time variable with Gaussian statistics. The drag force is velocity-dependent:

$$\mathrm{F}_{ij}^{(\mathrm{D})}(\mathrm{r}_{ij},\mathrm{v}_{ij}) = -\gamma w^{D}(r_{ij} * \mathrm{v}_{ij}) \quad (4)$$

where, $\mathrm{v}_{ij} = \mathrm{v}_{\mathrm{i}} - \mathrm{v}_{\mathrm{j}}$, $\mathrm{v}_i$and $\mathrm{v}_j$are the current velocities of the particles. We assume the common relationship between the drag and random force parameters

$$w^{D}(\mathrm{r}) = [w^{\mathrm{r}}(\mathrm{r})]^2 = (1 - \frac{r}{R_c})^{2} \text{ at } \mathrm{r} < \mathrm{R_c},\ w^{D}(\mathrm{r}) = 0 \text{ at } \mathrm{r} \geq \mathrm{R_c} \quad (5)$$

σ and γ are parameters that determine the level of energy fluctuation and dissipation; they are related as $\sigma^2 = 2\gamma k\mathrm{T}$ that allows to maintain constant temperature in the course of simulation via the Langevin thermostat. We assumed that γ = 4.5, a common value fitted to the diffusion coefficient of water.

Covalent chemical bonds are effectively represented by bonding potential binding beads together into chains. To maintain the chain integrity, neighbouring beads are connected by nearest neighbor bond (1-2) we use harmonic potential between neighboring beads to describe chain and bond rigidity. Harmonic (Hookean/Fraenkel) bond is defined by

$$U(r_{ij}) = \frac{\mathrm{K}_b}{2}(r_{ij} - r_0)^2 \quad (6)$$

where $r_{ij} = |\mathrm{r}_i - \mathrm{r}_j|$, r_0 is an equiblirium bond length and $\mathrm{K_b}$ is the bond rigidity, which is dependent on the bead type. Neighboring bonds are bound by harmonic angle potential to maintain chain structure. Potential is given by eq 7 :

$$\mathrm{U}(\Theta_{ijk}) = \frac{\mathrm{K}_\Theta}{2}((\Theta_{ijk}) - \Theta_0)^2 \quad (7)$$

Where is the θ_{ij} is the angle between the neighboring bonds equilibrium bonds, θ_0 is the equilibrium angle K_θ is the bond rigidity. Morse Potential bond is applied to depict the intermediate complex formation between transition metal and the ligands PVP and DMF which has been explained in detail in section 2.4.

2.2 DPD Models of PVP and DMF

Because we apply DPD to a particular practical system, an effort was made to create reasonable coarse-grained models of the polymer (PVP) and solvent (DMF). The solution is presented as a multicomponent mixture of beads of equal effective diameter R_c. PVP polymer has repeating unit of monomer N-vinylpyrrolidone (figure 1a). Each PVP monomer is dissected into three equal volume beads namely P,V and N beads $-\mathrm{CH_2CO}-$,$-\mathrm{CH_2CH_2}-$ and $-\mathrm{NCHCH_2}-$.

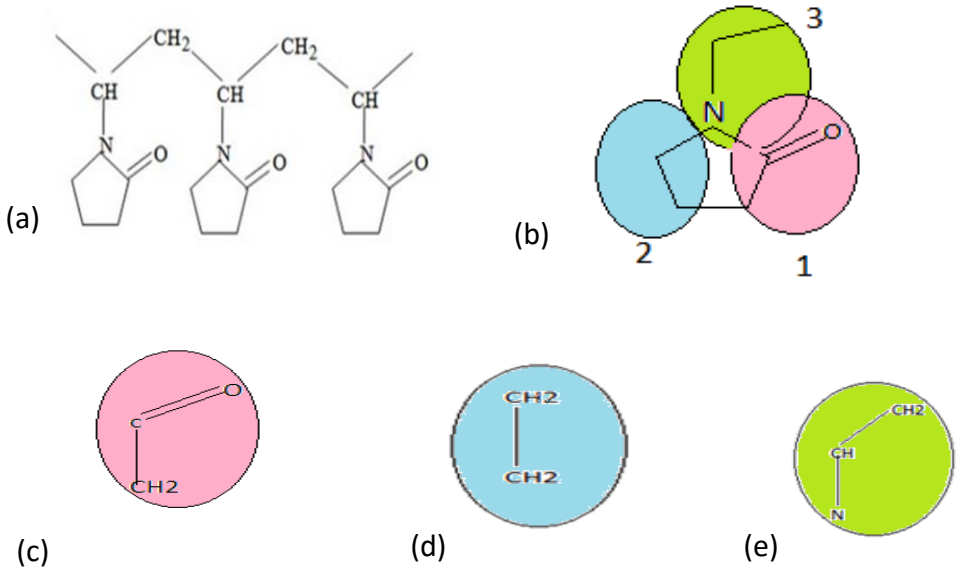

Figure 1: a) PVP polymer chain b) Schematic of coarse grained model of PVP. PVP represented as three different bead c) P, d) V and e) N.

DMF $(CH_3)_2NC(O)H$ is an common organic solvent. It was presented as D-E dimer (2 beads) representing –HNCHO–and $-\mathrm{CH_3CH}-$ fragments respectively (Figure 2). The total volume of DMF molecule allows 2-bead description very reasonable.

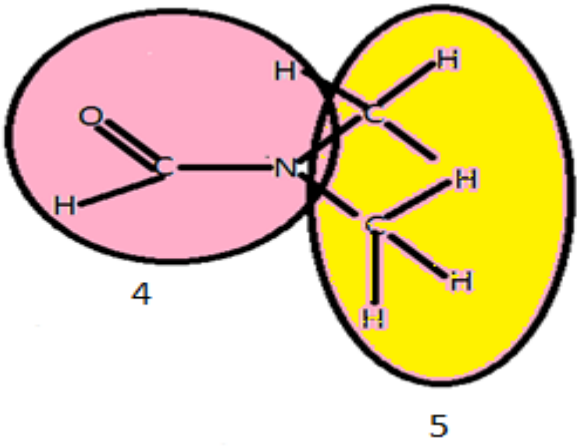

Figure 2:DMF coarse-grained model 4 and 5 denote D and E beads.

The volumes of the representative fragments were estimated using the effective volume parameters r_k of different functional groups taken from the Bondi [15] tables that are used in UNIFAC group-contribution model[16]. The parameters and the volumes of the beads are given in table 1. The volume of the beads were calculated using formula [18].

$$V = r_k * \frac{V_{VW}}{N_A}$$

Where V_{VW} is standard segement volume equals to 15.17 $\frac{cm^3}{mol}$ $N_A$and N_A is avagadro number.We can see that the volumes are nearly equal which justifies the use of single R_c value for all beads. We took 35 $Å^3$ of volume to calculate $Rc = (35 * 3)^{1/3} = 4.71$ Å.

Table 1: List of effective volume parameter, bead volume per mole and volume of bead.

Bead type	r_k $(\frac{cm^3}{mol})$	Vw $(\frac{cm^3}{mol})$	Volume of 1 bead $(Å^3)$
P	1.44	21.84	36.26
V	1.34	20.32	33.73
N	1.39	21.08	35
D	1.49	22.6	37.5
E	1.59	24.12	40.4

It should be noted that the beads are very small, much smaller than typical in DPD simulations. That is why the most common approach to obtaining the DPD bonded terms (fitting to atomistic simulations) is not fully applicable here: the resulting harmonic bonds will be too stiff. That is why we assigned a fixed spring constants to the bond parameters. The parameters of nearest neighbor (1-2) bonds for PVP molecule beads are determined by fitting the radial distribution functions for the conformations of coarse-grained chains to the results of atomistic MD simulations.

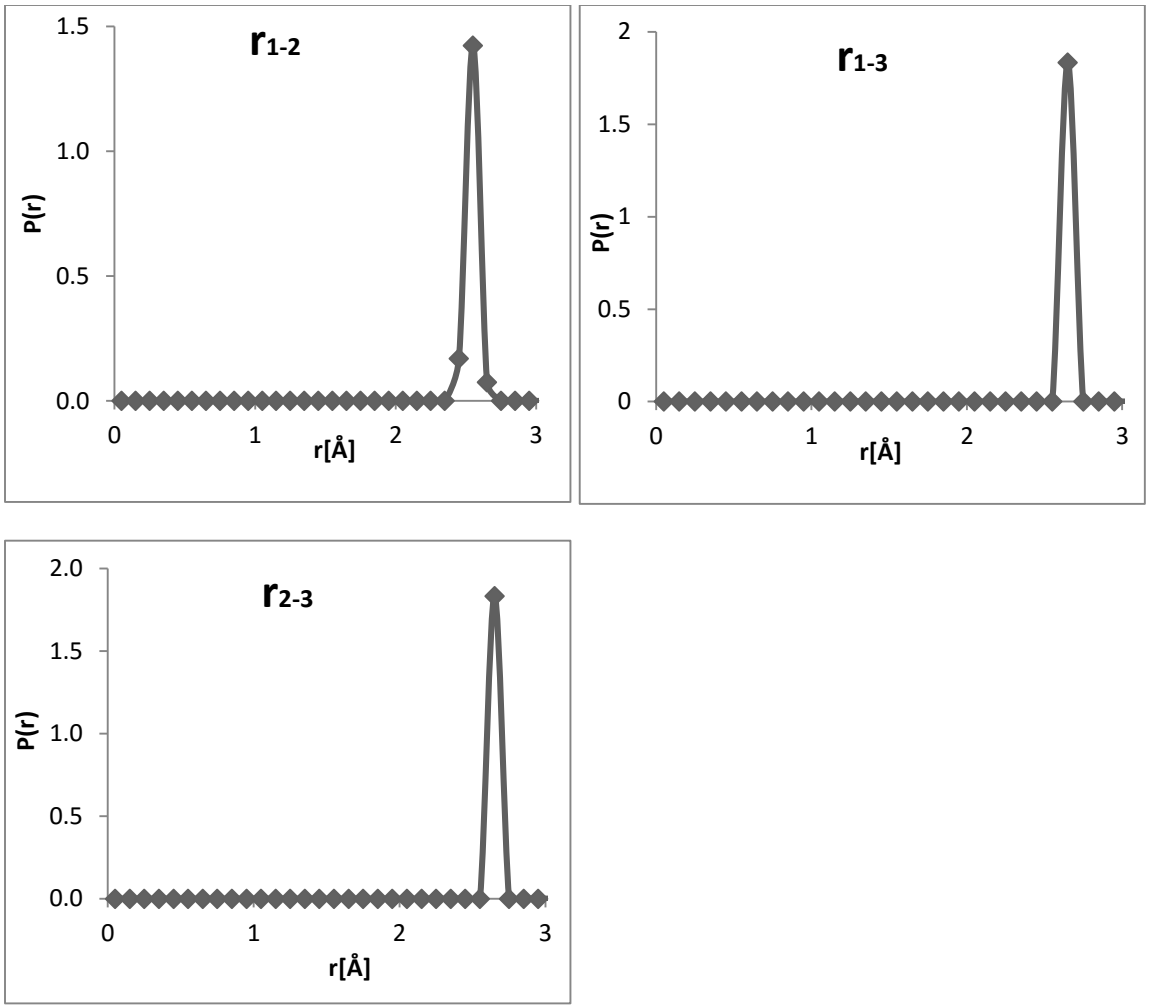

Figure 3: atomistic MD simulations at T = 298 K. The lines are obtained by MD simulations. The distribution of distances between the PVP beads are shown as in first plot r_{1-2} denotes distance between P and V beads. In second plot r_{1-3} denotes distance and third plot r_{2-3} distance between V and N beads.

2.3 Intracomponent repulsion parameter

Correlations between density, pressure and compressibility of single-component DPD systems were first obtained by Groot & Warren (GW) [17]. The equations that relate pressure, density and compressibility of the systems are given by GW

$$\frac{3}{R_C^3} = \frac{\rho}{\mathrm{MW}} N_A$$

GW determined the correlation between reduced dimensionless compressibility, density and the intracomponent repulsion parameter *a*

$$\kappa^{-1} = \frac{1}{nk\mathrm{T}k_{\mathrm{T}}}, \quad \kappa^{-1} = 1 + 0.2\alpha\rho/k\mathrm{T} \tag{8}$$

The pressure depends on the reduced density ($\rho/\mathrm{R_C^3}$) and repulsion parameter as

$$\mathrm{P} = \rho k\mathrm{T} + \alpha a\rho^2 \text{ , } (\alpha = 0.101 \pm 0.001) \tag{9}$$

Table 2: Bond parameters of PVP and DMF beads

	Fragment	Beads	Harm Bond	r_0[Å]	r_o/R_c	$\mathrm{K_b}(k\mathrm{T}/\mathrm{R_C^2})$
	CH2CO	P	P-V	2.55	0.51	320
PVP	CH2CH2	V	V-N	2.56	0.51	320
	NCHCH2	N	P-N	2.55	0.51	320
	NHCHO	D	D-E	1.94	0.39	440
DMF	CH3-CH2	E				
	Metal	C	A-C	1.88	0.4	320
	Coordination centre	A	C-C	3.10	0.66	320

Table 3: Interaction parameters for PVP, DMF and Metal chloride.

Bead type	Fragment	P	V	N	D	E	C	A	I
P	CH2CO	78.5							
V	CH2CH2	78.5	78.5						
N	NCH2CH2	78.5	78.5						
D	HNCHO	78.5	78.5	78.5					
E	CH3CH	78.5	78.5	78.5	78.5	78.5			
C		200	200	200	200	400	400		
A		0	0.0	0.0	0.0	0.0	0.0	0.0	
I		200	200	200	200	200	200	0.0	200

2.4 General concept: DPD model of transition metal and coordination bonds:

Metal ion is depicted as central atom C with coordination centers A around the central atom. We had to model the metal chloride in such a way that it has fixed number of coordination centers with rigid structure. Three different structure as shown in figure 4 are planar, tetrahedral and octahedral modeled as example. For planar structure we took one bead to represent the central metal ion and 4 coordinating centers in a plane at four corners of a square in the same plane. The bond angle is 90 degree. The planar geometry is maintained using straight A-C-A covalent angles. Similarly in the tetrahedral geometry, central atom is located at center with four substituents that are located at corners of a tetrahedron. The A-C-A bond angle is 109 degree. In case of octahedral six substituents are located at the vertices of octahedron around central atom bond angle of 90 degrees. Structure was kept rigid to obtain complex geometry. Harmonic bond rigidity taken is 320 $k\mathrm{T}/\mathrm{R}_{\mathrm{C}}^{2}$ between the beads to keep the bond intact. Bond Parameters has been given in table

3. We assigned very short ranged DPD repulsion for the C bead with all other beads (in general, the presence of complexi hardly influence the pressure and other properties in systems that do not contain any ligands). A beads only interacted with ligands via Morse potential. Therefore, intercomponent repulsion parameter $a_{AC} = 0$ and $a_{AA} = 0$ and $a_{CC} = 400$ k*T*/*R*c.

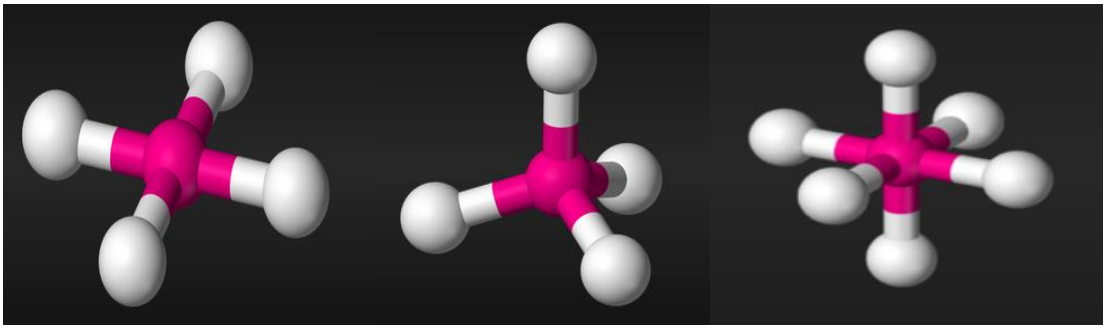

Figure 4: Coarse-grained models of complexi with planar, tetrahedral and octahedral molecular geometry. The central “metal” C bead is shown in pink, the coordination centers (A beads) are shown in white.

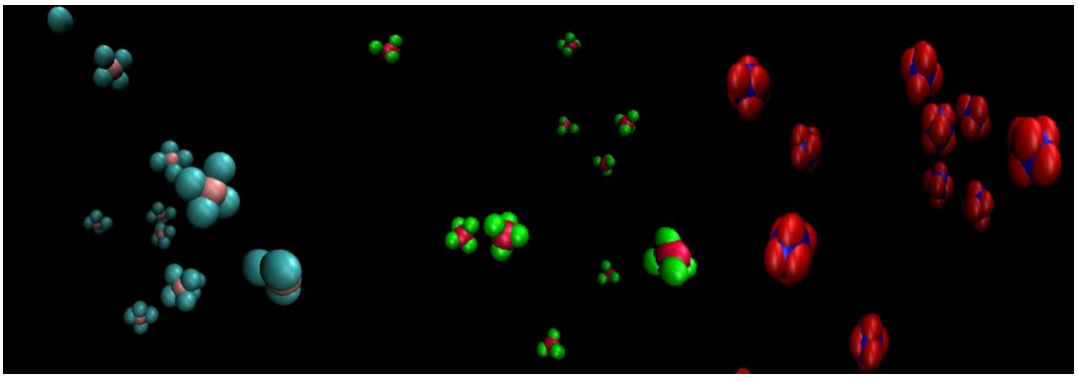

Figure 5: Configuration of planar , tetrahedral and octahedral beads.

Table 4: Bond parameters of planar , tetrahedral and octahedral beads.

Fragment	Bead	Harmonic bond	r_0/R_C	$K_b(\frac{kT}{R_C^2})$	Angle type	K_Θ	Equilibrium angle
Planar							
i) Metal	C	C-A	0.50	320	A-C-A	20	90
Coordination Center	A	A-A	0.707	320			
Tetrahedral							
ii) Metal	C	C-A	0.40	320	A-C-A	20	109
Coordination Center	A	A-A	0.66	320			
Octahedral							
iii) Metal	C	C-A	0.40	320	A-C-A	20	90
Coordination Center	A	A-A	0.56	320			

As the potential for the dissociable bonds, we applied the Morse interactions:

$$U^M(r_{ij}) = K_{ij}\{1 - \exp[\alpha_{ij}(r_{ij} - r_{ij}^0)]\}^2 - K_{ij}\{1 - \exp[\alpha_{ij}(r_{ij}^M - r_{ij}^0)]\}^2 \quad (10)$$

Where, K is potential strength,

α is potential width,

r^M is Morse radius,

r^0 is equilibrium length

The Morse force is

$$\mathrm{F}_{ij}^{(M)}(r_{ij}) = -2\alpha_{IJ}\mathrm{K_{IJ}}\exp\left[\alpha_{\mathrm{IJ}}\left(r_{ij} - r_{ij}^0\right)\right]\left\{1 - \exp\left[\alpha_{\mathrm{PB}}\left(\mathrm{r_{ij}} - \mathrm{r_{ij}^0}\right)\right]\right\}\mathrm{r_{ij}}/\mathrm{r_{ij}} \quad (11)$$

at $\mathrm{r_{ij}} < \mathrm{r_{ij}^M}$

Here the potential is cut and shifted is dependent on potential strength, Morse radius and potential width. In all our systems we assumed r^0=0 (that is, the minimum of potential is when the ligand location coincides with the coordination center). This makes possible to regulate the distance between the ligand and C bead using only one parameter $\mathrm{r}_{0(\mathrm{A-C})}$. The force is zero if r is greater than cutoff radius; otherwise attractive force keeps the bond associated. Parameters are decided based on the geometry of the beads. Figure 6 show how Morse plot actually looks and how energy changes as the Morse parameter is changed. Here the potential is cut and shifted and the overall depth depends upon all parameters where K is potential strength, α is potential width, r^{M} is Morse cutoff radius and r^0 is equilibrium length. How potential strength affects bond formation has been studied in section 3.1 .

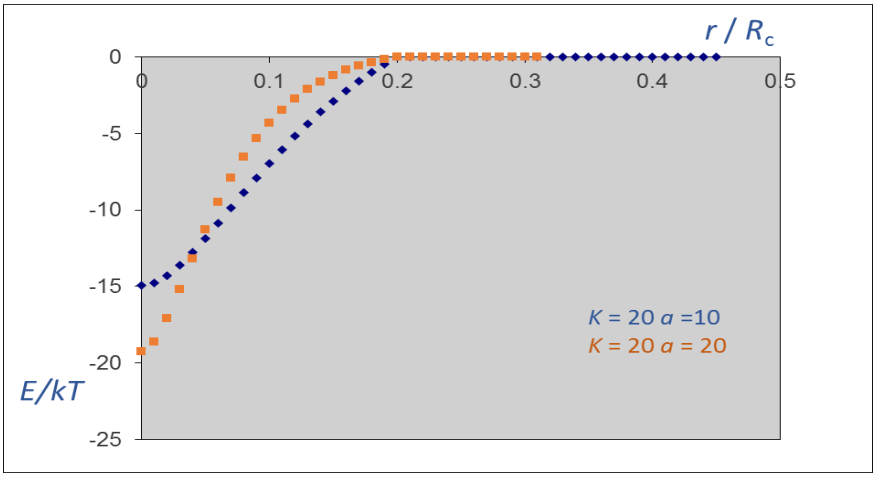

Figure 6: Cut-and-shifted Morse potential with 2 sets of parameters. K=20 and α=10, α=20, r_{0ij}=0, r_m =0.2Rc .

In our system we have PVP molecule, DMF as solvent and the metal chloride. Metal has four open coordination positions and two of them are occupied by chloride anion ligands making the complex electrostatically neutral. The remaining two positions are either occupied by carbonyl group of PVP or DMF. So Morse potential is applied between P bead of PVP and D bead of DMF with the A bead of metal chloride. The A-P and A-D bond formed dissociates as the distance exceeds $\mathrm{r_m}$ leading to breakup of the complex**.** Thus we adjust the parameters so that bond formed stays there for longer lifetime. Parameters of the bond selected are given in the table 4. In other section of thesis, we have adjusted the strength parameter accordingly and has been described there.

Table 5: Morse parameter for A-P and A-D potential

Fragment	a_{ij}	K	α	r_0	$\mathrm{r_m/R_C}$	R_C	ϒ
A-P	0.0	25	10	0	0.2	1	4.5
A-D	0.0	25	10	0	0.2	1	4.5

3 Properties of the model

In this section, we perform a general analysis of our approach. We check the ability of the model to qualitatively reproduce the desired phenomena it targets. First, we regulate the complexation using the depth of the Morse potential, and second, we model the equilibrium between several ligands around central metal ions.

3.1 Effect of Morse potential depth on complexation

As the first example, we considered solution of tetrahederal molecule with C as central atom, A taking tetrahedral position and 2 different types of beads namely P, D as ligands as mentioned above. Morse bond was applied between P and A beads. Thus complex compound was formed due to complexation of P and A beads. Various simulations were run and potential strength parameter K was varied from from 0 to 30. Other Morse parameters were taken as described in section 2.4 . Simulation was run for 2 million steps with time step of 0.01 . Box size of 10*10*10 $\mathrm{R_C^3}$ was taken. 1490 beads each of P and D beads were taken with 15 tetrahedral clusters representing the metal ions with total of 60 coordination center. So for 15 clusters we had total of 60 spots where ligands can form a bond.

As we mentioned before, we set $\mathrm{r_{0(P-A)}} = 0$ and $\mathrm{r_{m(P-A)}} = 0.2\mathrm{Rc} = 0.094\mathrm{nm}$. Thus the range of Morse interactions is very short, and approximately represents the actual range of 0.094 nm, so that the maximum distance at which the central atom and the ligand bead start interacting with each other is 0.282 nm. This approximately corresponds to the actual range of complex ion/ligand interactions. In Figure 7 we present the fraction of “filled coordination positions” that is the fraction of A beads that have a ligand P bead within distance $\mathrm{r_{m(P-A)}}$ from it. This fraction is plotted against K at fixed α. Because the potential is cut and shift, K does not really represent

the depth (like the classical, non shifted Morse potential). That is why, the fraction of filled centers is plotted twice, first against Morse potential having one ligand (figure 7) and second with actual Potential depth (figure 8).

The correlation between the depth and the filled fraction appear very reasonable.

3.1.1 Application to solution containing one ligand

We took system with 2 different types of beads namely P,D and also tetrahedral molecule with C as central atom and A taking tetrahedral position as described above. Morse bond was applied between P and C beads. Thus complex compound was formed due to complexation of P and C beads. Various simulations were done and potential depth K was varied from from 0 to 30 *k*T. Other Morse parameters were taken as described in section 2.4. We can see from the figure 7 that as the K value increases from 0 to 30 *k*T the no. of bonds formed between A and P beads was increasing and fraction of ligand occupying tetrahedral spot increases from 0 to almost 1 as K value approaches 20 *k*T and remains 1 as we increase it to 30 *k*T.

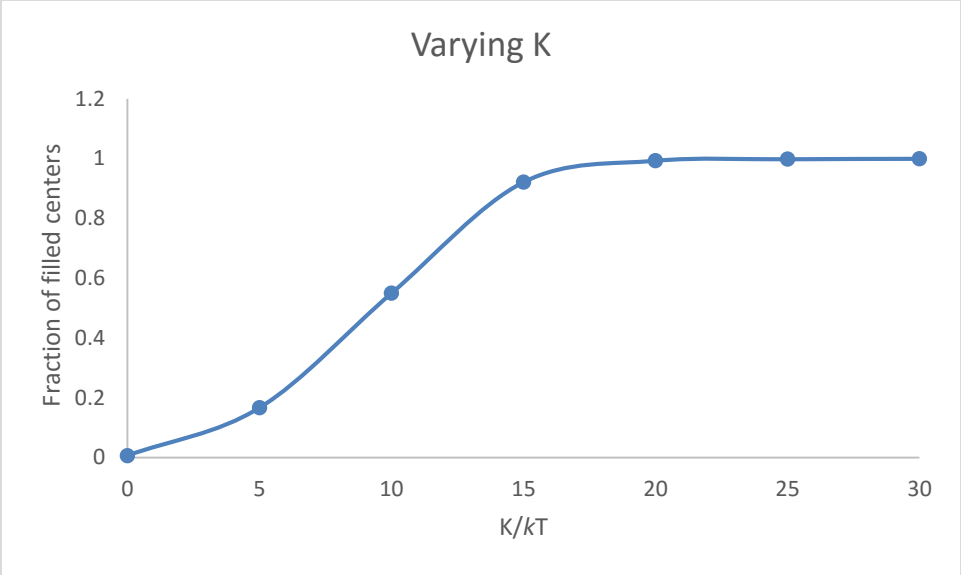

Figure 7: Fraction of tetrahedral spot occupied by P bead as Morse potential strength, K varies from 0 to 30 *k*T.

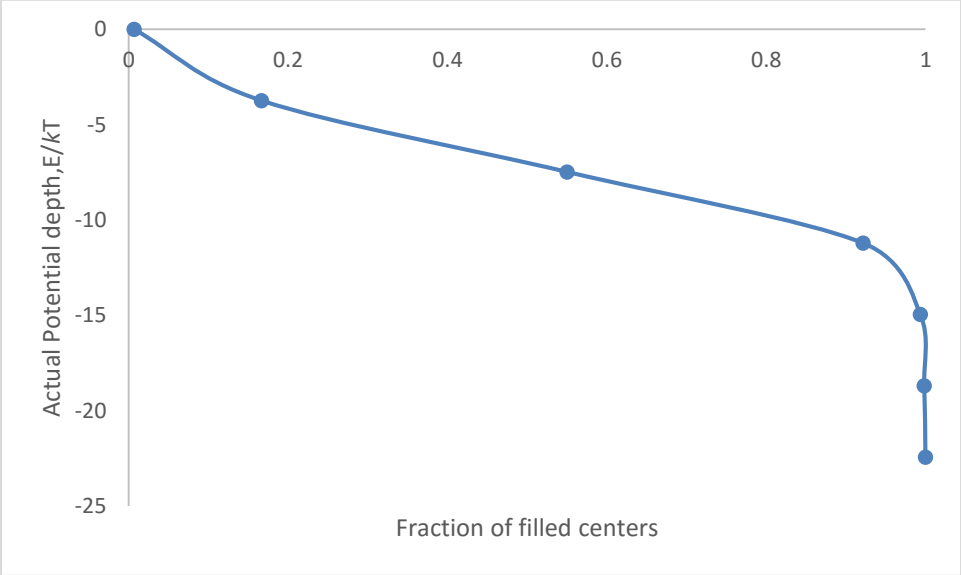

Figure 8: Actual Potential depth vs Fraction of Tetrahedral spot occupied P bead.

3.1.2 Application to solution with binary ligand mixture

Here we again took two different beads P and D with tetrahedral compound consisting of C as central bead and four coordinating center as A bead surrounding it. This time Morse bond was applied between both P bead and A bead as well as between D bead and A bead. Here we have taken two competing ligand and several simulations were run. For ligand P we have kept K as constant and equals 25 *k*T and for other ligand D it is gradually increased from 0 to 30 kT and we can see that as the potential depth increases from 0 to 25 *k*T, the bonds formed between D and A bead is increasing and it start competing with other ligand to occupy the tetrahedral spot. Again simulation was run for 2 million steps with time steps of 0.01. Box size of 10*10*10 Rc was taken. 1490 beads each of P and D beads were taken with 15 beads of tetrahedral compound with total of 60 coordination center. Figure 9 and 10 shows the fraction of filled centers plotted first against Morse potential strength having both the ligands and second with actual Potential depth .

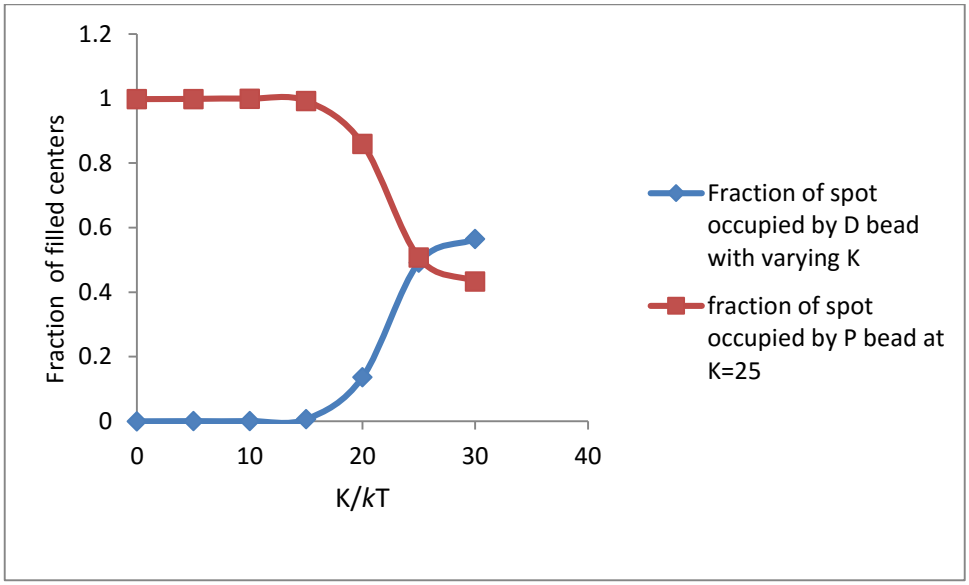

Figure 9: Fraction of tetrahedral spot occupied by P and D bead as Potential strength, K varies from 0 to 30 *k*T for D bead and K=25 *k*T for P bead.

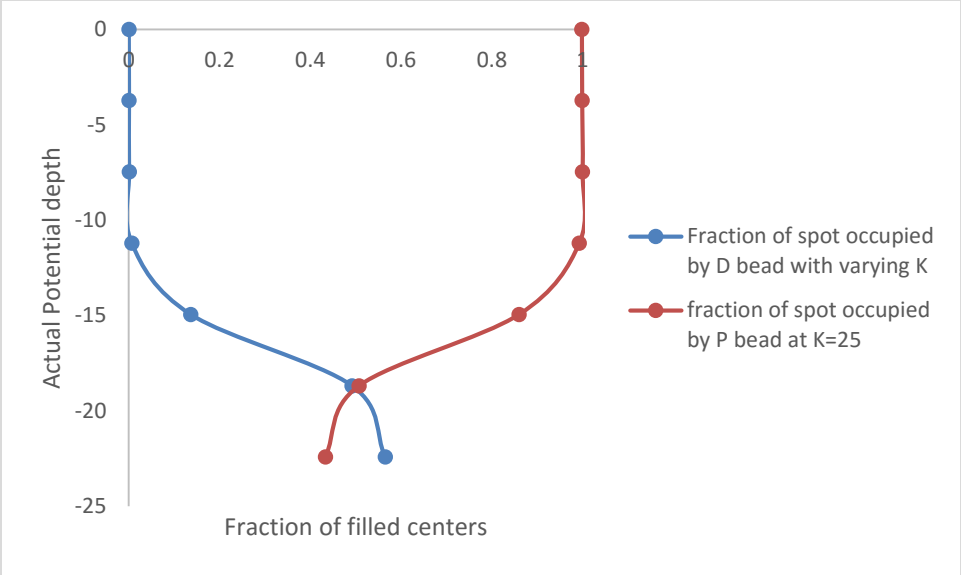

Figure 10: Actual Potential depth vs Fraction of Tetrahedral spot occupied by P and D bead.

As we see the model provides a reasonable picture: in the beginning, all coordination positions are occupied by P beads that are present in the solution. As the binding between the second ligand and the metal clusters strengthens, D beads start to compete with P beads for the coordination positions. This does not happen until $\mathrm{K_{A-D}}$ reaches about 17 *k*T. The Morse potential depth for A-D interaction is still 5.98 *k*T shallower than that of A-P interactions. As the difference in binding strength decreases, the share of coordination position occupied by P beads sharply increases to ½ at $\mathrm{K_{P-A}} = \mathrm{K_{D-A}}$=25 kT.

Overall, our approach qualitatively reproduces complexation of ligands around a complex metal ion. Without a great increase in computational expenses we achieved coordination of a correct number of ligands around metal atom in a desired geometry. By altering the Morse parameters, we have reasonably described processes that are observed during complexometric titration essentially based by displacement of a coordinated ligand by a stronger one. In the next chapter,

we apply the concept to a practical system, PVP–DMF solution with added transition metal chloride salt.

4 Application of DPD model of transition metal complexi to PVP-DMF-metal chloride solutions.

4.1 Target systems: review of experimental studies

Interaction between water soluble polymer and metal ions is important and has attracted great attention because of their intrinsic properties and their potential applications, such as superconducting materials, liquid crystals and biocompatible polymer [19, 20]. For our case we have chosen PVP which is neutral water soluble polymer. Both pure polymer and conventional coordination compound has different behavior than complexes consisting of polar polymer and metal ion. Researchers have great interest in PVP-metal complexes because of properties such as simple repeating unit, excellent solubility, and favorable biocompatibility and can be used as a model compound for proteins, a stabilizer for the synthesis of metal colloids, crystal morphology modifier of metal nanoparticles and also plays important roles in chemistry, biochemistry and pharmaceutical science, such as highly efficient catalysts. Through that work, people tried to understand interaction between metal ions and PVP in solution . From their results it was found that apparent viscosity increases as we keep adding metal in PVP-DMF as solution. When metal ions are coordinated to two or more different carbonyl group, the coordination sites act as crosslinking points among PVP chains which are entangled. This causes increase in apparent molecular weight and molecular weight distribution which weakens the mobility of the polymer[21].

The target of this chapter is to demonstrate that using our model we are able to provide at least a qualitative description of a complex practical system that is well studied experimentally. The complexation of PVP monomer around metal ions is most clearly manifested in dynamic

properties of PVP and its solutions that change qualitatively due to coordination bond formation between the metal cations and monomers when metal chlorides are added to solutions of PVP. In particular, the apparent viscosity of PVP-Metal chloride-DMF solution depends both on the concentration of added metal chloride and the nature of the metal ion. Figure 13 shows the dependence of dynamic viscosity of the shear rate for three different metals and fixed concentration. LiCl causes only a very moderate increase in viscosity since Li+ has practically no ability to coordination. But complex forming bivalent Ca^{2+} and Co^{2+} have much more pronounced effect, most visible for $CaCl_2$. The coordination bonds form between the cation and the carbonyl group in the lactam ring. Main reason behind the differences in apparent viscosity for different metal ion is because of the differences in the coordination structure between metal ions and the carbonyl group determined by the ionic radius, electric charge and electronic structure. More the coordination no., more will be the crosslinking. Similarly larger ionic radius means there is more room for ligands. For ions with smaller radius, steric hindrance is strong that results in less affiliation of carbonyl group of PVP towards the metal ion. Lesser macroligands coordinated to metal ions will result in reduction in crosslinking[21].

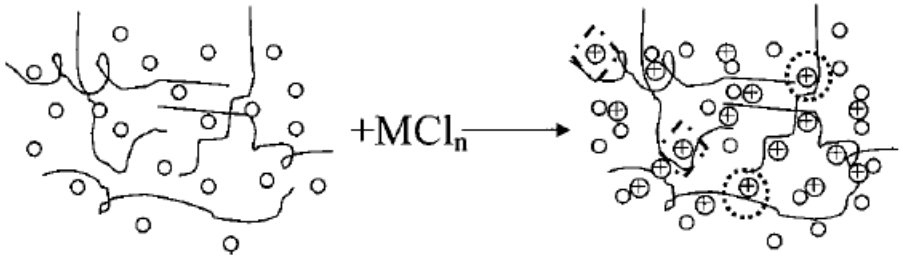

Figure 11: Schematic illustration of the aggregation state of PVP in the presence of MCl_n. The open and crossed circles represent DMF molecules and M_{n+} ions, respectively. The rhombus dots and circular curves represent intrachain and interchain interactions.

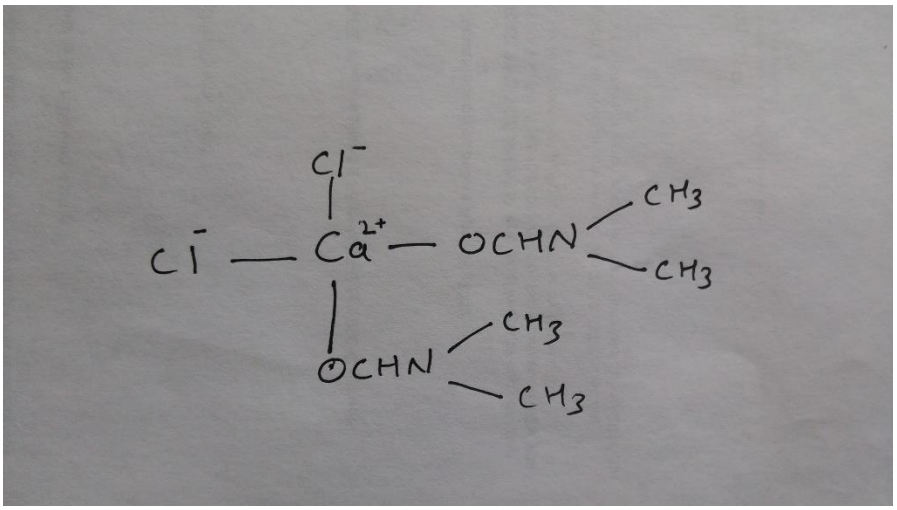

Figure 12: Chemical scheme of a complex consisting of Ca^{2+}, two Cl atoms and 2 DMFs connected to Ca via carbonyl oxygens.

Metal ion has open coordination positions where two of them are occupied by chloride anion ligands making the complex electrostatically neutral. The two other positions are either occupied by carbonyl group of PVP or DMF. Figure 12 shows the chemical scheme of the complex consisting Ca^{2+}, two Cl atoms and 2 DMFs.

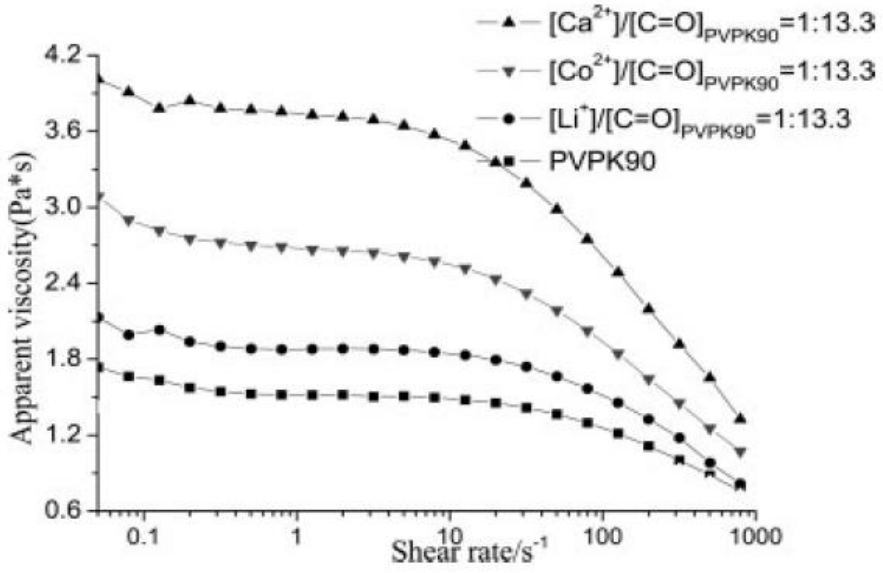

Figure 13: Rheological curves of the apparent viscosity of concentrated PVPK90 solutions containing different metal chlorides at the same concentration.

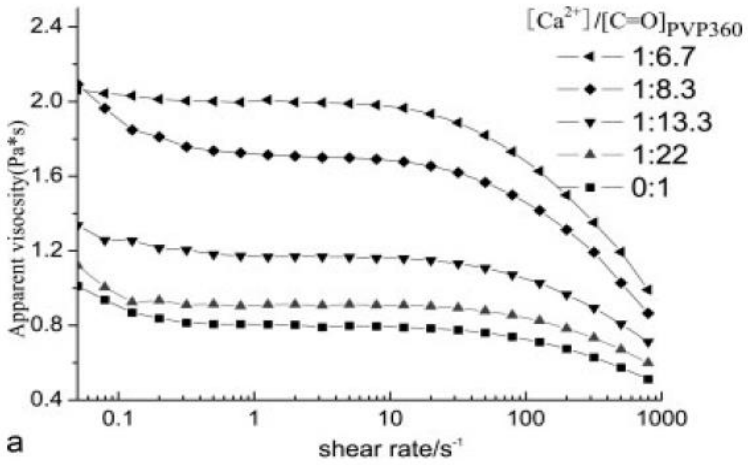

Figure 14: Apparent viscosity of concentrated PVP solutions versus the shear rate in PVP– $CaCl_2$– DMF system for different $CaCl_2$ concentrations.

5 DPD studies of dynamic properties of PVP-DMF-metal chloride solutions

In order to determine the viscosity, we simulated in a slit channel formed Poiseuille flow. If the walls are parallel to *xz* plane and a constant gravity-type field is applied to every bead of the fluid, a liquid-like system establishes a parabolic velocity profile. The dependence of the average velocity of the beads on the position in *x* direction is described with the following equation:

$$v_y = \frac{\rho g_y (xD - x^2)}{2\eta} \qquad (12)$$

Where η is the dynamic viscosity, ρ is the mass density, g_z is the gravitational constant, *x* is the position between the walls, D is the distance between the plates[22]. This equation allows evaluation of the dynamic viscosity η from the velocity profile, if the latter can be reasonably fitted with parabolic equations.

We studied how concentration affects the viscosity of the PVP-DMF solution then we studied how viscosity changes as polymer length changes. It has been described in section 5.1.2. Then we studied what is the effect of Morse potential parameter K on the viscosity of system which is described in section 5.1.3. After that we studied how driving force affects the Poiseuille flow of the system and viscosity which is described in section 5.1.4.

5.1.1 Viscosity as function of concentration of metal chloride

On the first step, we examine the role of metal chloride concentration on the dynamic properties of the solution. The simulations were set up as follows: We took PVP polymer, DMF as solvent and metal chloride in the system to study how real system behave as the concentration of metal chloride is increased. Metal ion complexes are formed between lactam ring of PVP and metal chloride and also between DMF and metal chloride in the solution. We took PVP polymer with 60

monomer per chain in DMF solvent. Each PVP monomer has been trisected into three beads namely P, V, N and each DMF bead as D and E beads as described in section 2.2. And metal chloride is depicted as one central bead 'C' having tetrahedral structure with 2 spots occupied by chloride ion represented by 'I' bead and other two spots for coordination bond formation which is represented by 'A' beads. The Bonding between chloride and the metal ion is permanent with harmonic bond rigidity of 320 $\frac{k\mathrm{T}}{\mathrm{R_C^2}}$. And dissociable bond is formed between the ligands and the coordination center by applying modified Morse potential. Interaction parameters are given in table 3. Model of tetrahedral metal ion is described in section 2.4. Simulation was carried out in 30*30*30 $\mathrm{R_c^3}$ cell. 270 molecules of PVP bead and 16200 beads of DMF solvent is taken in the system. And thus we have equal no. of P and D beads. No. of metal chloride beads is varied from 0 to 10,000 beads i.e. from 0 to 2285 $(\frac{\text{no. of } \mathrm{MCl_2} \text{ beads}}{(\text{no.of PVP monomer})}) * 10^{-8}$ per $\mathrm{R_C^3}$. Simulation was run for 0.2 million steps with time step of 0.01. Walls of frozen particles are added to the surfaces orthogonal to *x* axis of thickness $4\,\mathrm{R_c}$ on both sides projecting a slit channel. In our implementation of Poiseuille flow (as it is set up in DL_MESO[23]) , the walls consist of implicit beads distributed uniformly with density $5/\mathrm{R_C^3}$. A Constant body force of 0.004 (DPD units) in the direction of y-axis is added to each non-frozen particle which gives Poiseuille flow of the DPD fluid. Repulsive parameter for walls is set to $a_{ii} = 78.0\ k\mathrm{T}/\mathrm{Rc}$ and $a_{ij} = 50.0\ k\mathrm{T}/\mathrm{Rc}$. DPD beads of the confined fluid can overlap with the walls. Velocity profiles plotted are shown in Figure 16. They have nearly zero velocity, due to the drag force acting between the confined polymer/solvent beads and the implicit wall beads. Strong fluctuations in this region are due to very low density in the region of wall-fluid overlap. Closer towards the center, at about the wall position, the average velocity rises step-wise. This means that the simulation setup does not provide a no-slip condition at the walls (no-slip condition was obtained for single-bead fluid). The

remaining portion of the profile towards the center is parabolic. By regression analysis of the y-velocity profile obtained from the simulation, we get the equation of parabola. As for example, curve obtained for system with 50 metal chloride was fitted with equation $y - 0.4222 = -0.0002x^2 + 0.007x$ (Figure 15). This parabolic equation is equated to equation 12 to get viscosity. In similar fashion, viscosity was estimated for different concentration of metal chloride in the PVP-DMF solution. As we have mass density of 3 and gravitational constant applied equals to 0.004 .

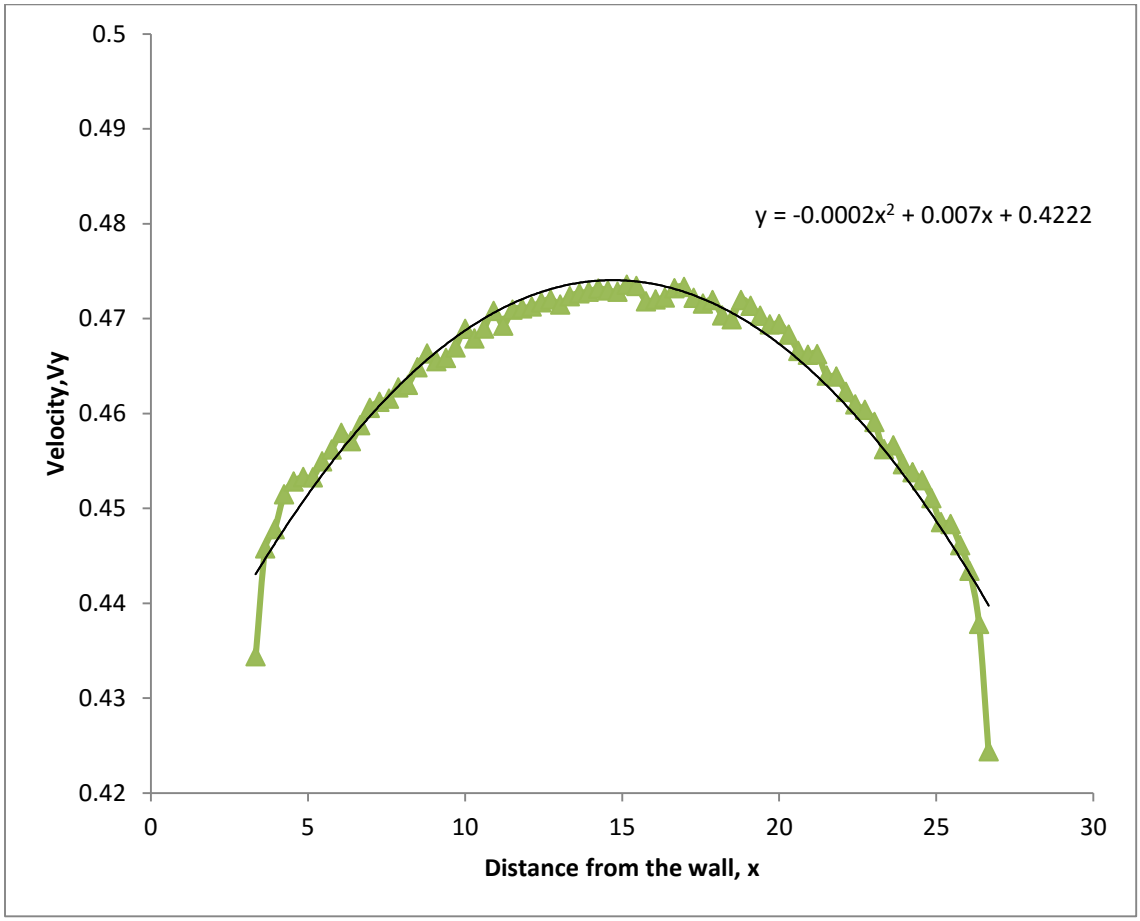

Figure 15: Velocity profile for PVP-DMF-metal chloride solution in a slit-shaped pore with the driving field of 0.004 (DPD units) for the concentration of 11.48 $(\frac{\text{no. of } MCl_2 \text{ beads}}{(\text{no.of PVP monomer})}) * 10^{-8}$ per R_C^3.

The velocity profiles become “shallower” as the MCl_2 concentration increases, obviously leading to higher viscosity (Figure 17), similarly to the experiments. Yet, the parabolic shape of the profile remains fairly pronounced until the concentration reaches 228.5 $(\frac{\text{no. of } MCl_2 \text{ beads}}{(\text{no.of PVP monomer})}) * 10^{-8}$ per R_C^3 . Above that concentration, we observe essentially flat velocity profiles in the central part. Thus, the fluid becomes a single flexible body moving in direction of the flow. The velocity is constant due to the balance of the driving field and the friction between the fluid and the wall.

Overall, the model qualitatively reproduces the experimental picture: when two or more carbonyl groups from different PVP molecules are coordinated to one metal ion simultaneously, coordination site can act as crosslinking points or bridges among the entangled PVP chains, which increases the molecular weight. More metal chloride in solution means more bond formation which weakens the mobility of the molecular chains. This results to increase in viscosity of the fluid which is similar to what has been found experimentally. The phenomenon is qualitatively suitable for the test of the model, because the crosslinking bonds are not permanent; they have a finite strength (can be broken with effort) and even in undisturbed state they have a finite lifetime. That is why metal chloride (just as in the experiment) does not convert PVP into a classical cross-linked network. The strength of the coordination crosslinking bonds depend on a metal and there the dependence of the viscosity on the metal originates from.

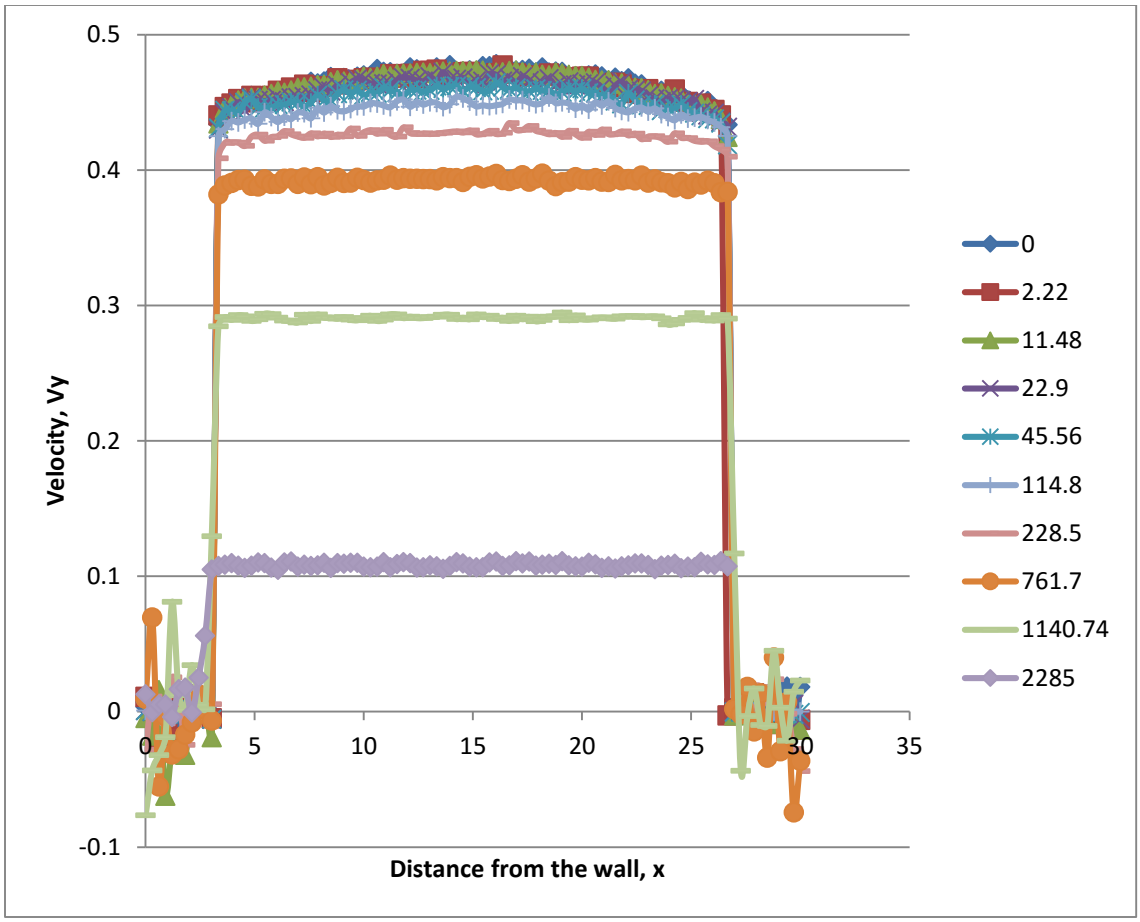

Figure 16: Velocity profile of the fluid at different metal chloride concentration. Unit of concentration is in $\frac{\text{no. of } MCl_2 \text{ beads}}{(\text{no.of PVP monomer})} * 10^{-8}$ per R_C^3.

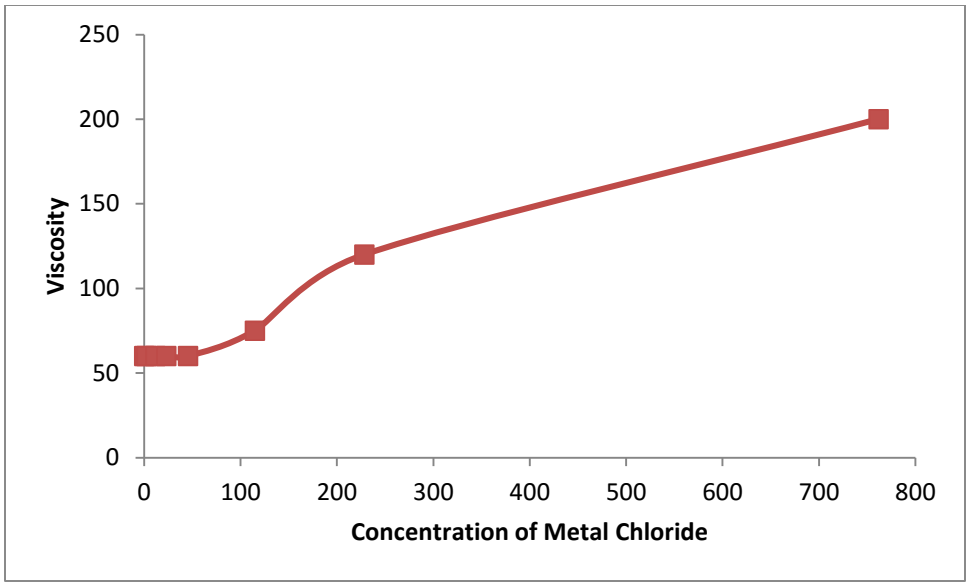

Figure 17: Viscosity as a function of concentration of metal chloride in system of DMF solvent and PVP polymer. Unit of concentration is in $\frac{\text{no. of } MCl_2 \text{ beads}}{(\text{no.of PVP monomer})} * 10^{-8}$ per R_C^3.

5.1.2 Viscosity as a function of Polymer length

Then we studied how polymer length affects the viscosity of a fluid. First we took only PVP polymer to study as an example. Number of monomers per chain of molecule of PVP was varied from 1, 5 , 10, 20,40 to 60. So for polymer with 60 chains have total of 180 beads with each of 60 P, V and N and accordingly for other polymer length chains. Box size of 30*30*30 R_c^3 was taken with total no. of 81000 beads. Simulation was run for 0.2 million steps with time step of 0.01. All the bond and interaction parameter selected has been described in section 2. Then again we ran set of simulations, this time with PVP polymer and tetrahedral structure C representing central bead with four 'A' beads at tetrahedral positions. Box size of 30*30*30 R_c^3 was taken. Total no. of beads taken was 81,000. And 200 beads of tetrahedral compound was taken with 800 coordinating spots where ligand can associate to form bond. Viscosity was calculated using

equation 12 from the velocity profile obtained by curve fitting as explained in previous section. Velocity profile in figure 18 shows that as the length of monomer per chain increases, velocity distribution becomes more and more flat. And logarithmic graph was plotted with viscosity on y-axis and length of polymer chain on x-axis. As we can see in figure 19, viscosity of the system increases as the polymer chain length increases. And it has also been observed that system with metal ion has slightly higher viscosity.

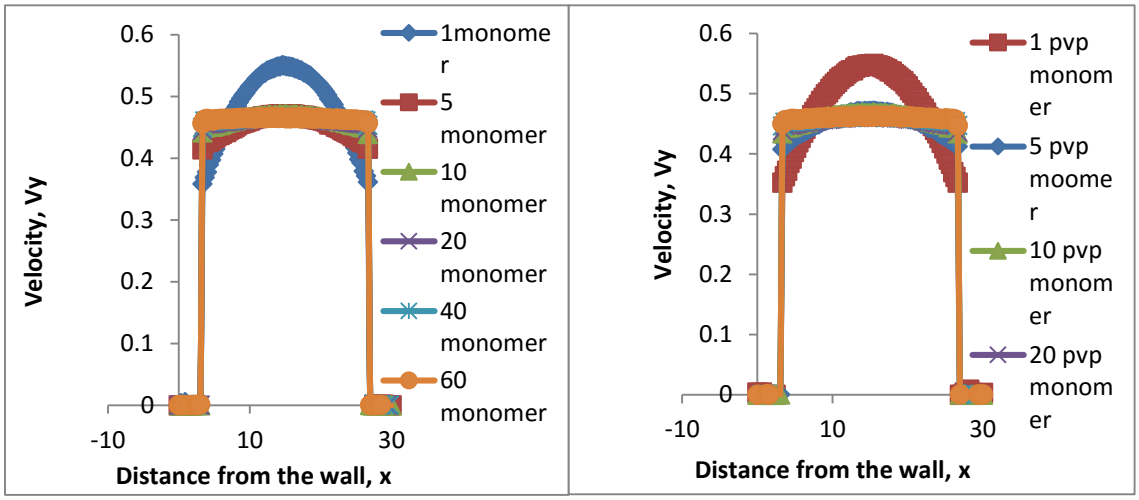

Figure 18: Velocity profile with different polymer chain length. i) only PVP and ii) PVP-Tetrahedral particle without Cl.

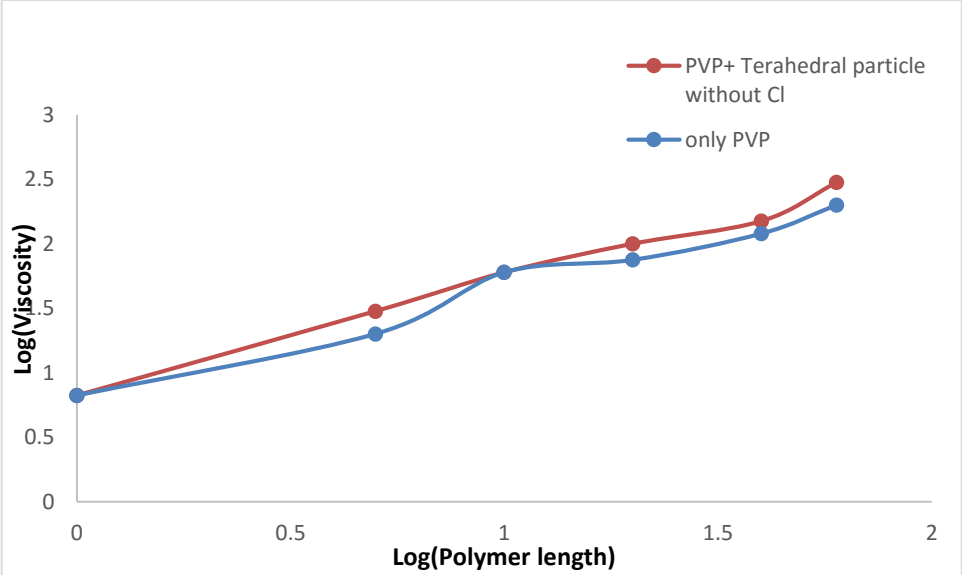

Figure 19: System containing only PVP with varying polymer chain length (in red) and system containing PVP and tetrahedral particle without chloride ion(in blue).

Again some more simulations were run, this time with system containing PVP polymer and DMF solvent with tetrahedral structure compound . Box size again was 30*30*30 R_C^3. 81,000 of total beads were taken, out of which 20250 DMF beads were there . And 200 beads of tetrahedral shape particles were taken with 800 coordinating spots where both the ligands of PVP and DMF can attack. Simulation was run for 0.2 million steps with 0.01 time step. After that another set of simulations were run for PVP-DMF-metal chloride system. Again Box size of 30*30*30 R_c^3 was taken. Total no. of beads taken was 81,000. 16200 beads of DMF solvent is taken in the system. And 200 beads of tetrahedral shape bead was taken with 400 coordinating spots where ligand can attack. Other 400 spots out of 800 were occupied by chloride ion represented as 'I' bead. Again velocity profile were drawn from simulation results (figure 20) and viscosity was calculated. Similar results were found. As the polymer chain length increases viscosity (figure 21).

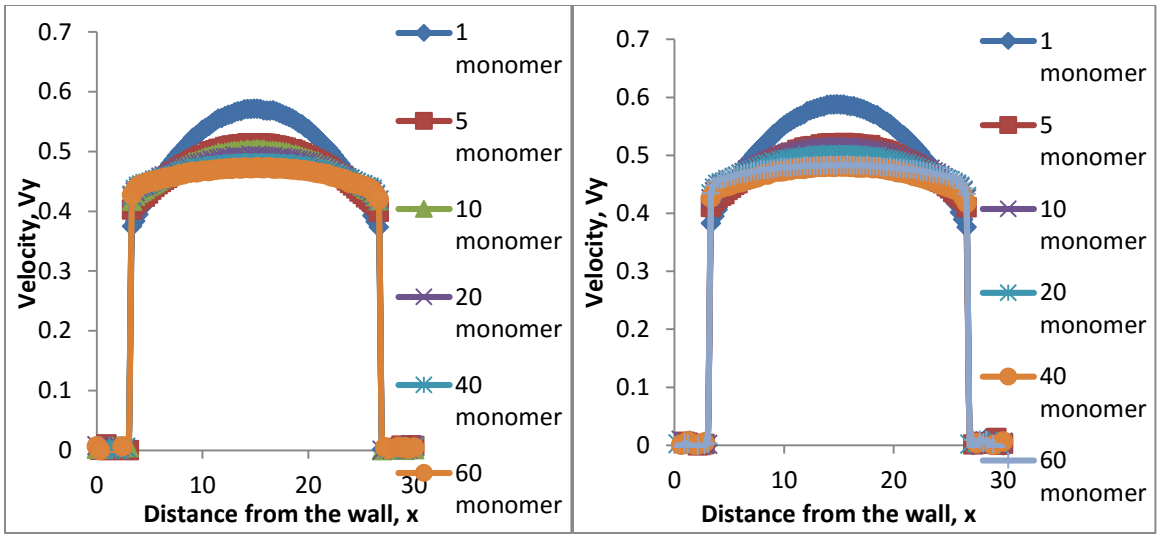

Figure 20: Velocity profile for PVP-DMF-Tetrahedral compound with and without chloride of different polymer chain length.

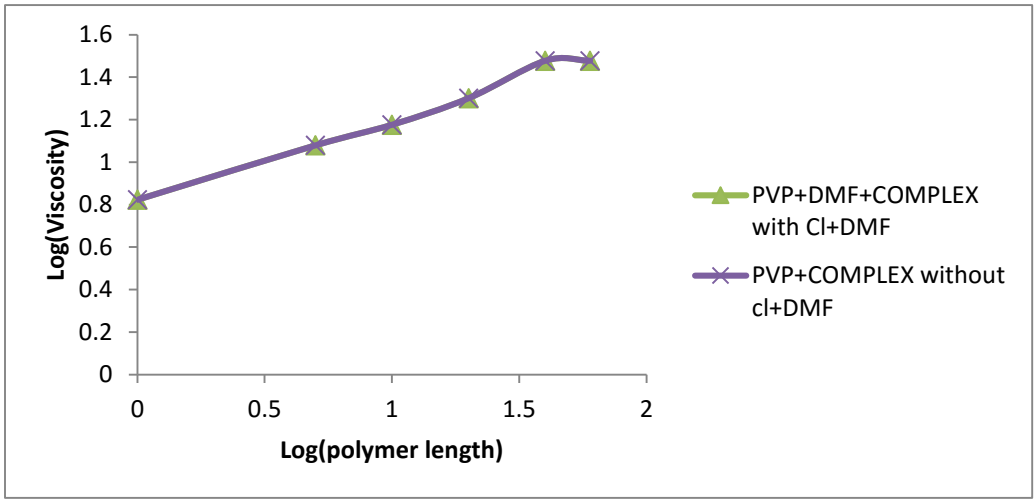

Figure 21: Logarithmic viscosity vs Logarithmic polymer length trend for PVP, DMF and metal chloride system with and without Cl.

It can be inferred from the graphs that polymer chain length affects the flowability of the fluid. Longer the polymer chain more viscous the system will be. Longer polymer chain forms more entangled structure. For longer chain polymers, one metal ion may get coordinated to different carbonyl group of different PVP polymer which act as a crosslinking bridge which causes the fluid to be more viscous. These quantitative results shows that length of polymer chain affects the flowability of fluid and viscosity is higher for polymers with longer chains.

5.1.3 Viscosity as a function of Morse potential parameter K

Here we studied the effect of Morse potential, K on viscosity of real system. We took PVP and metal chloride with box size of 30*30*30 R_c^3 . Total no. of beads taken was 81,000. And 200 beads represented by 'C' with four beads at tetrahedral position represented by 'A', making total of 800 tetrahedral positions. 400 spots out of 800 were occupied by chloride ion represented by 'I' bead. Remaining 400 spots were acting as coordination center where ligands can attack to form dissociable bond. Simulation was run for 0.2 million steps with time step of 0.01. All the bond and interaction parameters taken are explained in section 2. Morse bond was applied between P bead of PVP and A bead of tetrahedral metal chloride. Morse potential parameter K was varied from 0 to 5, 10, 15, 20, 25 to 30. All other Morse parameters are taken as described in section 2.4. Velocity profile plotted yet again (figure 22) to see how it varies with Morse potential strength. And viscosity was calculated as described before (figure 23). Viscosity was found to be more or less same with little variation. It shows the flow property is not much affected just by varying the Morse potential parameter K. Velocity profile remains in same range with variation of K.

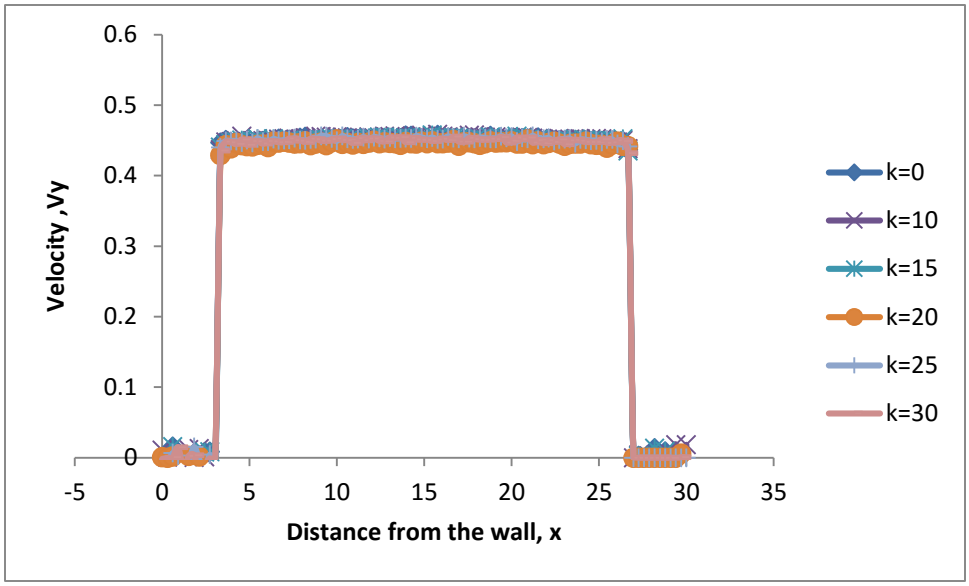

Figure 22: Velocity profile at different Morse potential depth, K for PVP-metal chloride system.

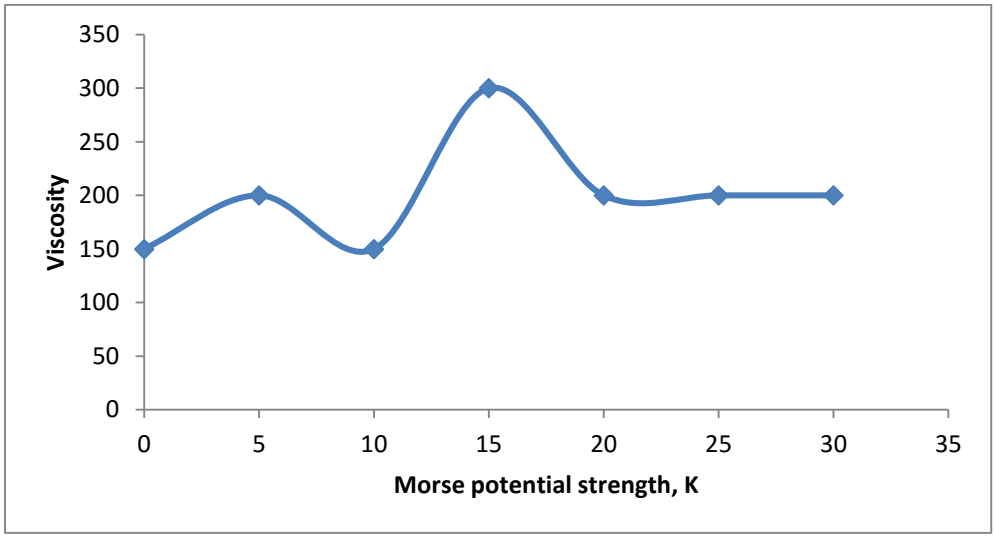

Figure 23: Viscosity with Morse parameter variation. System contains PVP and metal chloride

5.1.4 Viscosity as a function of driving force

In this case, for our real system with PVP-DMF-metal chloride, we studied if the force applied on the fluid affects its velocity profile and viscosity. We applied driving force within the the range of 0.001 to 0.009. Again Box size of 30*30*30 R_c^3 was taken. Total no. of beads taken was 81,000. 16200 beads of DMF solvent is taken in the system. And 200 beads of tetrahedral shape bead was taken with 400 coordinating spots where ligand can attack. Other 400 spots out of 800 were occupied by chloride ion represented as 'I' bead. From the Poiseuille flow obtained, viscosity was calculated using equation 12 again by curve fitting. We found that for the system on which higher driving force was applied were flowing at higher velocity but nature of the velocity profile was similar in shape (figure 24). And the velocity gradient was more or less same for all the system irrespective of the driving force. We can infer from the results that a fluid will flow at higher velocity if we increase the driving force but the relative velocity or the velocity gradient is not much affected which causes the viscosity of the fluid to be same.

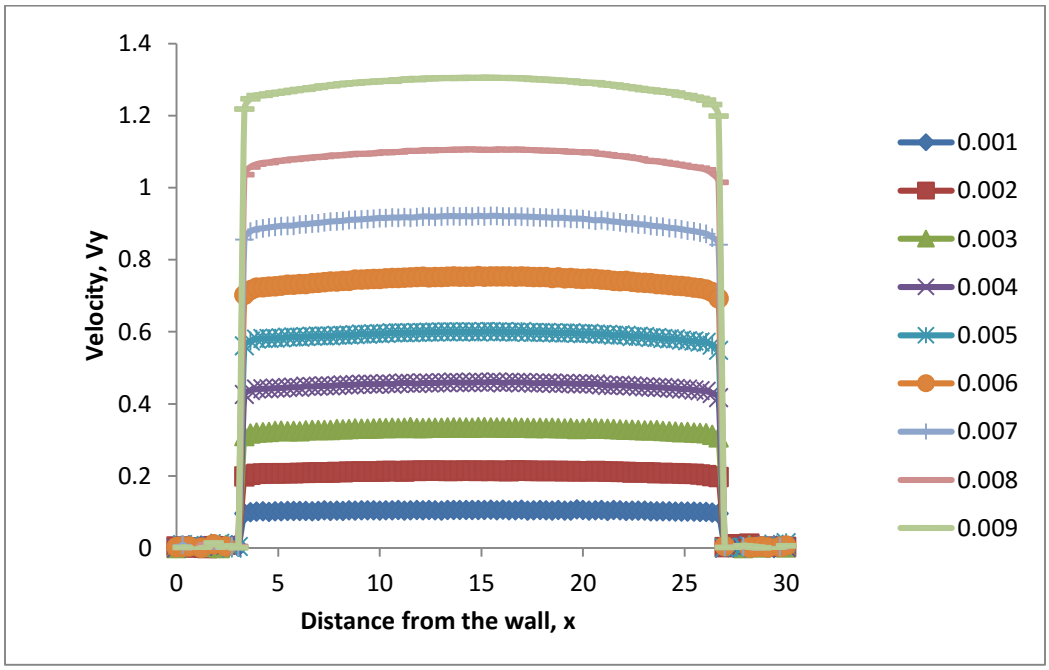

Figure 24: Velocity profile at different driving force applied. Driving force is in DPD units.

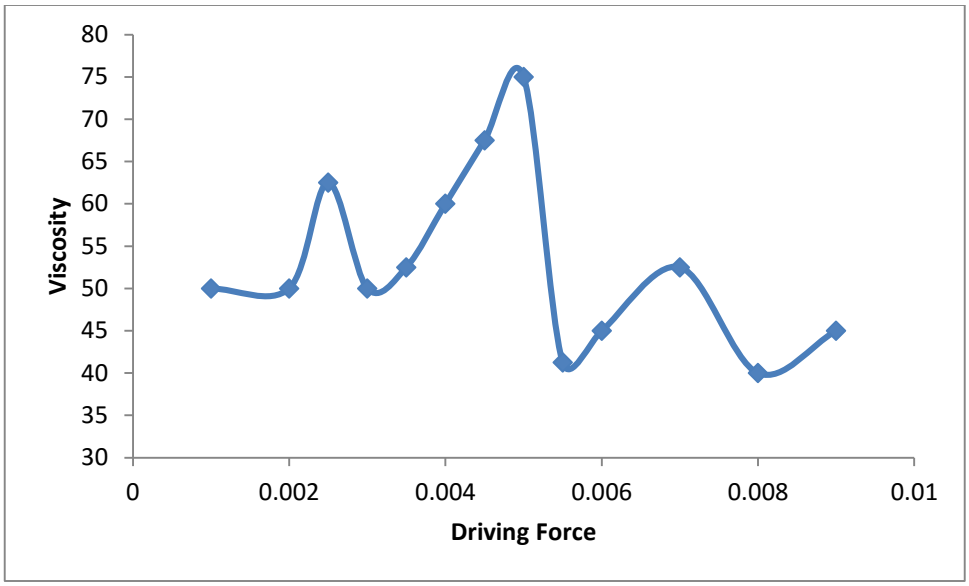

Figure 25: Viscosity of PVP-DMF-Metal chloride system at different driving forces.

Thus we see from the results that a fluid will flow at higher rate if we increase the driving force but the relative velocity or the velocity gradient is not much affected which causes the viscosity of the fluid to be same (figure 25).

6 CONCLUSION

This work presents an extensions of a methodology for mesoscale simulations of systems with reactive equilibria to solutions that include transition metal cations that can coordinate ligands. Unlike reactive systems considered previously, transition metal cations (1) have fixed number of open coordination positions (2) these positions are arranged in a fixed geometry (or several possible fixed geometries, e.g. square and tetrahederal). To overcome this difficulty, we presented cations not by individual beads, but by clusters of beads. Each cluster contains the central bead to which other beads are attached. Those beads represent coordination positions. Using systems of harmonic bond and angle constraints, we maintain the desired geometric arrangement of coordination position beads corresponding to the actual geometry of complexes around the metal ion that we want to model. In order to describe chemical equilibria, the coordination interactions were described with cut and shifted Morse potential applied between each coordination centre and a ligand. We employed DL_MESO package[23] for all the DPD simulations, which is an openly distributed code.

Preliminary studies demonstrate feasibility of simulations of transition metal cations. We did reproduce complexes of desired geometries in DPD. The number of coordination bonds formed proved sensitive to the Morse parameters. In a model system with two different ligand types, we obtained a qualitatively reasonable picture of replacement of one ligand with another as the bonding between the replacing ligand and the coordination centers strengthened. Yet, it remains unclear how the Morse parameters should be fitted to any particular ion-ligand pair. Simulations with the Morse depth of potential equal to the actual strength of the coordination interactions are hardly feasible: the lifetime of the coordination bond in simulations will be comparable with the simulation time. The unavailability of the actual depth should not discourage, since DPD

potentials are generally artificial. Yet, at this point we offer no recipe for choosing the Morse parameters to any particular system.

Our attempt to model a practical system (PVP solution in DMF with added $CaCl_2$) gave mixed results. In that system, metal has four open coordination positions and two of them are occupied by Cl^- anion ligands. This makes the complex electrostatically neutral. The bonding between the two remaining coordination positions of the metal and carbonyl groups of DMF and PVP (with PVP being a stronger ligand) affects the dynamic properties of the system: it makes PVP chains reversibly crosslinked. Although we did qualitatively reproduce viscosity increase in the system as the metal chloride was added and, eventually, a transition from viscous to elastic behavior, other aspects of the experimental behavior of the solution (such as dependence of viscosity on the strength of Morse potential did not reproduce well.

Yet, overall, our modelling study advances methodology of mesoscale simulations of reactive systems.

REFERENCES

1. Nikunen, P., I. Vattulainen, and M. Karttunen, *Reptational dynamics in dissipative particle dynamics simulations of polymer melts.* Physical Review E, 2007. **75**(3).
2. Groot, R.D. and T.J. Madden, *Dynamic simulation of diblock copolymer microphase separation.* Journal of Chemical Physics, 1998. **108**(20): p. 8713-8724.
3. Gavrilov, A.A., Y. V. Kudryavtsev, P. G. Khalatur, A. V. Chertovich, *Microphase separation in regular and random copolymer melts by DPD simulations.* Chemical Physics Letters. **503**(4-6): p. 6.
4. Wu, S., T. Lu, and H. Guo, *Dissipative particle dynamic simulation study of lipid membrane.* Front. Chem. China, 2010. **5**(3): p. 11.
5. Yan, K., Y.Z. Chen, J. Han, G.R. Liu, J.S. Wang, N.G. Hadjiconstantinou, *Dissipative particle dynamics simulation of field-dependent DNA mobility in nanoslits.* Microfluidics and Nanofluidics, 2012. **12**(1-4): p. 157-163.
6. Vishnyakov, A., D. Talaga, and and A.V. Neimark, *Simulation of Protein Conformations with DPD: from a-helices to b-structures.* Journal of Physical Chemistry Letters, 2012. **3**: p. 7.
7. Lisal, M., J.K. Brennan, and W.R. Smith, *Mesoscale simulation of polymer reaction equilibrium: Combining dissipative particle dynamics with reaction ensemble Monte Carlo. I. Polydispersed polymer systems.* Journal of Chemical Physics, 2006. **125**(16).
8. Lisal, M., J.K. Brennan, and W.R. Smith, *Mesoscale simulation of polymer reaction equilibrium: Combining dissipative particle dynamics with reaction ensemble Monte Carlo. II. Supramolecular diblock copolymers.* Journal of Chemical Physics, 2009. **130**(10).
9. Karimi-Varzaneh, H.A., P. Carbone, and F. Mueller-Plathe, *Fast dynamics in coarse-grained polymer models: The effect of the hydrogen bonds.* Journal of Chemical Physics, 2008. **129**(15): p. 10.
10. Nikoubashman, A., R.A. Register, and A.Z. Panagiotopoulos, *Sequential Domain Realignment Driven by Conformational Asymmetry in Block Copolymer Thin Films.* Macromolecules, 2014. **47**(3): p. 1193-1198.
11. Svaneborg, C., *LAMMPS framework for dynamic bonding and an application modeling DNA.* Computer Physics Communications, 2012. **183**(8): p. 1793-1802.
12. Lee, M.T., A. Vishnyakov, and A.V. Neimark, *Modeling Proton Dissociation and Transfer Using Dissipative Particle Dynamics Simulation.* Journal of Chemical Theory and Computation, 2015. **11**(9): p. 4395-4403.
13. Lee, M.T., A. Vishnyakov, and A.V. Neimark, *Coarse-grained model of water diffusion and proton conductivity in hydrated polyelectrolyte membrane.* Journal of Chemical Physics, 2016. **144**(1): p. 12.
14. Groot, R.D., *Electrostatic interactions in dissipative particle dynamics-simulation of polyelectrolytes and anionic surfactants.* Journal of Chemical Physics, 2003. **118**(24): p. 11265-11277.
15. Bondi, A., *van der Waals volumes and radii.* The Journal of physical chemistry 1964. **68**: p. 11.
16. Hansen, H.K., P. Rasmussen, A. Fredenslund, M. Schiller, and J Gmehling, Industrial & engineering chemistry research. **30**(24): p. 2352.

17. Groot, R.D. and P.B. Warren, *Dissipative particle dynamics: Bridging the gap between atomistic and mesoscopic simulation.* Journal of Chemical Physics, 1997. **107**(11): p. 4423-4435.
18. Santiago, R.S. and M. Aznar, *Liquid-liquid equilibrium in ternary ionic liquid systems by UNIFAC: New volume, surface area and interaction parameters. Part II.* Fluid Phase Equilibria, 2011. **303**(2): p. 111-114.
19. Tsuchida, E. and H. Nishide, Advance Polymer science, 1977. **24**(1).
20. Higashi, F., C. S. Cho, and H. Kakinoki, Polym Sci Polym Chem Ed 1979. **17**(313).
21. Hao, C.W., Zhao, Y., Zhou, Y., Zhou, L. J., Xu, Y. Z., Wang, D. J., Xu, D. F., *Interactions between metal chlorides and poly(vinyl pyrrolidone) in concentrated solutions and solid-state films.* Journal of Polymer Science Part B-Polymer Physics, 2007. **45**(13): p. 1589-1598.
22. Backer, J.A., Lowe, C. P., Hoefsloot, H. C. J., Iedema, P. D., *Poiseuille flow to measure the viscosity of particle model fluids.* Journal of Chemical Physics, 2005. **122**(15).
23. Seaton, M.A., R.L. Anderson, S. Metz, and W. Smith, *DL_MESO: highly scalable mesoscale simulations.* Molecular Simulation, 2013. **39**(10): p. 796-821.